Не реферир (Труды конф).

PROCEEDINGS REPRINT

SPIE—The International Society for Optical Engineering

Reprinted from

Gamma-Ray and Cosmic-Ray Detectors, Techniques, and Missions

5–7 August 1996
Denver, Colorado

Сокращ. след. образом

1) T.G. Guzik et al.; in Gamma-Ray, and Cosmic Ray Detectors, Techniques, and Missions, B.D. Ramsey and T.A. Parnell, Editors, SPIE Proceedings, 2806, 122 (1996)

2) E-S. Seo et al., in Gamma и т.д. 2806, 134 (1996).

SPIE PROCEEDINGS SERIES

Volume 2806

The Advanced Thin Ionization Calorimeter (ATIC) Balloon Experiment: Instrumentation

T. G. Guzik[1], J. H. Adams Jr.[3], G. Bashindzhagyan[4], O. V. Dudnik[7], S. Ellison[1], A. R. Fazely[5], L. Garcia[5], N. L. Grigorov[4], S. E. Inderhees[9], J. Isbert[1], H. C. Jung[6], L. Khein[4], S. K. Kim[6], R. A. Kroeger[3], R. Lockwood[1], F. B. McDonald[2], M. I. Panasyuk[4], C. S. Park[6], B. Price[1], W. K. H. Schmidt[8], C. Dion-Schwarz[3], V.G. Senchishin[7], E.-S. Seo[2], J. P. Wefel[1], J. Z. Wang[2], V. I. Zatsepin[4], and S. Y. Zinn[2]

[1]Department of Physics & Astronomy, Louisiana State University, Baton Rouge, LA, USA
[2]Institute for Physical Science & Technology, University of Maryland, College Park, MD, USA
[3]Naval Research Laboratory, Washington, D.C., USA
[4]Skobeltsyn Institute of Nuclear Physics, Moscow State University, Moscow, Russia
[5]Department of Physics, Southern University, Baton Rouge, LA, USA
[6]Department of Physics, Seoul National University, Seoul, South Korea
[7]Department of Physics & Technology, Kharkiv State University, Kharkiv, Ukraine
[8]Max Planck Institut für Aeronomie, Katlinberg - Lindau, Germany
[9]Universities Space Research Association, Washington, DC, USA

ABSTRACT

A new balloon instrument, the Advanced Thin Ionization Calorimeter (ATIC), is currently under development by an international collaboration involving researchers in the US, Germany, Korea, Russia and the Ukraine. The instrument will be used, in a series of long duration balloon flights, to investigate the charge composition and energy spectra of primary cosmic rays over the energy range from about 10^{10} to 10^{14} eV. The ATIC instrument is designed around a new technology, fully active Bismuth Germanate (BGO) ionization calorimeter that is used to measure the energy deposited by the cascades formed by particles interacting in a ~1 proton interaction length thick carbon target. The charge module comprises a highly segmented, triply redundant set of detectors (scintillator, silicon matrix and Cherenkov) that together give good incident charge resolution plus rejection of the "backscattered" particles from the interaction. Trajectory information is obtained both from scintillator layers and from the cascade profile throughout the BGO calorimeter. This instrument is specifically designed to take advantage of the existing NASA long duration balloon flight capability in Antarctica and/or the Northern Hemisphere. The ATIC instrumentation is presented here, while a companion paper[1] at this conference discusses the expected performance.

1. INTRODUCTION

The ATIC project includes researchers from the US (Louisiana State University, University of Maryland, Naval Research Laboratory, Southern University), Europe (Moscow State University, Max-Planck Institut für Aeronomie, Kharkiv (Ukraine) State University) and Korea (Seoul National University) who are focused on investigating the energy spectra of Galactic Cosmic Rays (GCR) in the ultra-high-energy (> 10^{12} eV) regime. Cosmic rays are the product of energetic processes in the galaxy, and their interactions with matter and fields are the source of much of the diffuse gamma-ray, x-ray, and radio emission that we observe. In addition, these high energy particles are the only sample of matter from distant regions of the galaxy, and possibly elsewhere in the Universe, that can be directly observed by space experiments in the Solar System. Understanding cosmic ray origin and acceleration, and how they propagate, is a fundamental problem which has a major impact on our understanding of the universe.

Cosmic ray matter contains all natural elements from Hydrogen to beyond Nickel. All species have similar energy spectral shapes, power laws beyond ~10 GeV/nucleon, where the effects of heliospheric modulation become small. This power-law describes the spectra over an enormous energy range, to >10^{14} eV. All-particle measurements (where the species charge can not be distinguished), principally from ground-based air shower arrays, have traced the spectrum to the highest energies, ~10^{20} eV. From these measurements, it has been known for some time that the spectrum is somewhat steeper above 10^{16} eV than it is below 10^{14} eV. Whether and how this structure, the famous "knee", is related to the mechanisms of acceleration, propagation, and confinement is one of the major current questions in particle astrophysics.

0-8194-2194-4/96/$6.00

Over the past 15 years, theorists have developed an attractive and convincing theory of diffusive shock acceleration by supernova blast waves that naturally accounts for the essential observed features of most of the relativistic particles in the galaxy. It is a characteristic of diffusive shock acceleration that the resulting particle energy spectrum is much the same for a wide range of parameters, or shock properties. This energy spectrum, when corrected for leakage from the galaxy, is consistent with the observed power law spectrum of galactic cosmic rays (GCR). The maximum energy to which astrophysical shocks can accelerate particles is dependent upon the rate at which particles diffuse back and forth across the shock (i.e. on the magnetic field) and the time that the shock remains effective at accelerating particles. For the conditions thought to apply to supernova generated shocks, this limit is somewhere between Z x 10^{14} eV and Z x 10^{16} eV, where Z is the particle charge, depending upon assumptions about the magnetic field topology[2,3]. This implies that at energies starting around 10^{14} eV, where few measurements are available, we may expect to see the GCR relative composition change and the spectra steepen as the supernova acceleration mechanism is replaced by another source. Thus, this theory of cosmic ray acceleration may explain the "knee" structure observed in the all-particle spectrum, and makes definite predictions that can be tested by direct measurements at high energies.

The ATIC balloon flight program will concentrate on measuring the cosmic ray proton and Helium spectra from about 10^{10} eV to more than 10^{14} eV, with statistical accuracy better than 30% at the highest energy. This unique coverage of, at least, four orders of magnitude in energy with a single instrument will approach the energy range of previous experiments which concluded that a bend exists in the proton spectrum[4,5,6,7]. Most significantly, our measurements will be able to verify whether the proton and Helium spectral differences that have been reported from combining all the existing data are indeed real[3]. In addition, the ATIC results will fill an existing gap in measurements of the proton/Helium ratio between the traditional "standard" measurements below 100 GeV (e.g. Ryan et al.[8]) to the highest emulsion chamber energies. Concurrently, the ATIC flights will also measure the spectra of heavy nuclei up to iron, with individual element resolution and superior energy resolution.

In this paper, we discuss the experimental details of the ATIC instrument and balloon payload. A companion paper[1] at this conference provides further information on the ATIC scientific justification and results of simulations designed to investigate the expected instrument performance.

2. EXPERIMENT TECHNIQUE

To accomplish its scientific goals, the ATIC instrument must be capable of measuring the charge and energy of incident cosmic rays over an energy range from 10^{10} to $>10^{14}$ eV. The most practical method of energy determination for cosmic ray nuclei from H-Fe over such an energy range is ionization calorimetry. In an ionization calorimeter, a particle's energy is deposited inside an absorber via a cascade of nuclear and electromagnetic interactions. At each step, the energy of the primary particles is sub-divided among many secondary particles. Ultimately, the primary energy is dissipated via ionization and excitation of the material. The integral of the deposited energy over the depth in the absorber is a measure of the energy of the incident hadron. In principal, an infinitely deep absorber will provide energy resolution limited only by the statistical nature of the cascade process and the measuring technique. However, the resolution of a finite calorimeter depends on the fluctuations in the energy transferred to neutral pions that decay to the gammas initiating the electromagnetic cascade.

Practical calorimeters for space and balloon applications are necessarily limited in absorber thickness in order to have a reasonable mass and geometrical factor for collecting the particles. An optimized thin calorimeter experiment would have a target as thick as possible in interaction lengths, to force interactions of both the incoming primary and secondary hadrons, while remaining thin in terms of radiation lengths, so the cascade development occurs not in the target but in the calorimeter. The calorimeter should be thick in terms of both radiation lengths, to absorb the cascades, and interaction lengths, to force additional interactions of the particles. An optimal calorimeter material fulfilling most of these conditions is Bismuth Germanate, BGO. It has both a short radiation length as well as a short interaction length due to its high Z components and its high density. BGO is a relatively hard, rugged, non-hygroscopic scintillation crystal which does not cleave and does not show any significant amount of self-absorption of its scintillation light. By using BGO crystals the ATIC calorimeter can be made to be (essentially) fully active.

In a calorimeter experiment, there are particles "back-scattered" from the calorimeter into the charge measuring detectors[9,10]. Simulations confirm that as the proton energy increases, the number of "back-scattered" particles per unit area

increases, potentially adding to the charge signal of the incident cosmic ray and degrading the ability to distinguish between protons and Helium. To address this problem, ATIC incorporates a triply redundant charge module which includes a Silicon-matrix, a directional Cherenkov and a segmented scintillator hodoscope. Both the Silicon-matrix and Cherenkov detectors are composed of discrete "pixels" to reduce the sensitive area of any single sensor and, therefore, decrease the probability that a pixel hit by the incident cosmic ray will also be hit by back-scattered particles. Using these detectors, simulations indicate that, at 1 TeV, <2% of the incident cosmic rays would be subject to possible charge misidentification[1].

3. THE ATIC APPARATUS

3.1. Instrument Detectors

A schematic drawing of a "strawman" design for the ATIC instrument is shown in Figure 1. The instrument is composed of two major subsystems: the target module and the calorimeter. The target module consists of a Silicon Matrix array (Si), a segmented Cherenkov detector (Ck), two layers of plastic scintillator at the top (S1) and bottom (S3) of a stack of four 10 cm thick carbon targets with a third scintillator layer (S2) mid-way in the carbon stack. The total thickness of the carbon (40cm) is a little more than one interaction length (38.1cm) and somewhat more than two radiation lengths (18.8cm). Thus, more than 60% of the incident particles will interact somewhere in the target, but the showers created in the interactions, even at the very top of the target, would still be very "young" when they enter the calorimeter.

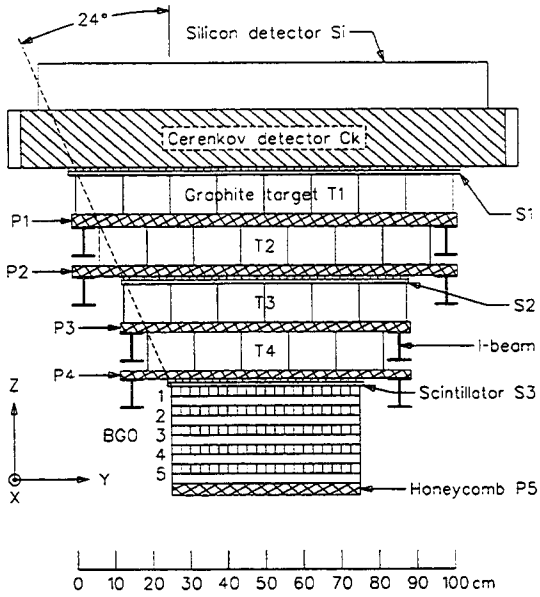

Figure 1: The ATIC "strawman" instrument.

The calorimeter module is composed of about 400 closely packed BGO crystals arranged in 10 layers, with each layer having an area of 50 x 50 cm^2. Alternating layers are placed at right angles to provide trajectory information. The total thickness of the calorimeter will be more than sufficient to contain the average shower maximum from electromagnetic particles created in 10^{14} eV proton interactions in the target.

The ATIC instrument has a geometrical factor of about 0.23 m^2-sr. Assuming that at least 10 particles in the highest energy bin have their first interaction in the target module, it is possible to achieve the near-term objectives of simultaneously measuring the proton and Helium spectra up to 10^{13} eV in a nominal one-to two-day "turn-around" flight. The exposure needed to reproduce or refute previous controversial results will require 3-4 LDB flights in Antarctica.

3.1.1. The BGO Calorimeter

The ATIC calorimeter consists of a "package" of 400 BGO crystals, each of which has dimensions 2.5 cm by 2.5 cm by 25 cm. With BGO, the shower "converter" and ionization detector are one and the same, enabling a close packed array of crystals to form a calorimeter that is active, where most of the deposited energy is converted into a detectable signal.

Figure 2 shows a side view of the assembled calorimeter looking along the X axis. Each pair of layers forms one XY plane with 80 BGO crystals held in one tray that is attached to the structure of the gondola. Each tray is fitted with handles at the corners for ease of transport as well as disassembly in the field. The BGO subunits (the BGO crystals with their readout device attached) are mounted on a steel plate with shock absorbing silicone rubber between the steel and the crystals. The subunits are held in place in each plane by steel "fingers" extending from the top to the bottom plate between the readout devices at the end of the subunits. To prevent the crystals from moving horizontally, the sides of the bottom steel plate are bent upward and fastened to the top plate. The arrangement for the Y subunits is identical, and both X and Y subunits are fastened together to form the XY unit. The front end electronics modules (FEMs) are attached either on the sides of the tray or in the corners.

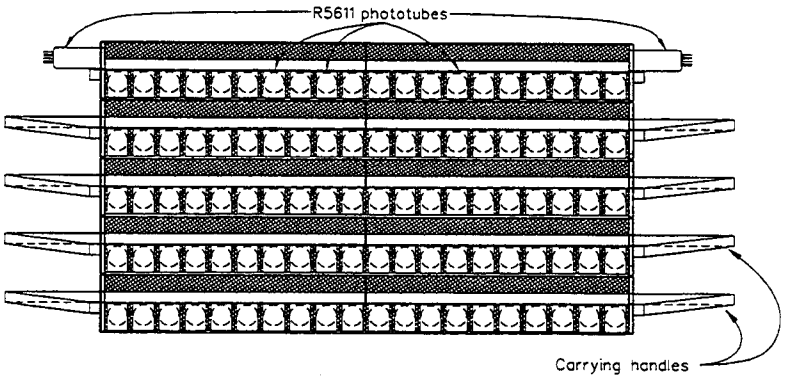

Figure 2: Side View of the assembled calorimeter.

The total thickness of the calorimeter is about 25 cm, corresponding to 22.3 radiation lengths and 1.12 interaction lengths of BGO. Adding the structural material gives a total of 22.8 radiation lengths and 1.29 interaction lengths. This is more than sufficient to contain the average shower maximum in 10^{14} eV proton interactions in the target. At the same total energy, Helium and heavier nuclei would produce lower energy electromagnetic cascades compared to those produced by protons. All the secondaries produced in the target, as well as the surviving primary, would have a ~70% probability of interacting further in the thick BGO calorimeter. The photon cascades from these BGO interactions would quickly convert in the BGO crystals, thereby further improving the energy resolution.

Figure 3 shows a cross section of a BGO subunit. Each crystal is wrapped in Teflon tape, 40μm thick, and covered with copper or brass foil, 25μm thick, for light tightness and RF shielding. The crystals are read out by a Hamamatsu R5611-01 photomultiplier tube (PMT) glued onto one end, with its base directly attached to it. A light attenuator (developed black & white negative film) is glued between the PMT and the crystal to keep the readout linear over the entire expected signal range. A light emitting diode (LED) is mounted onto the side of the PMT for calibration and liveliness tests.

According to our simulations, about 30-40% (depending weakly on energy) of the incident particle energy is deposited in the calorimeter. However, the energy deposit fluctuates over a wide range starting from particles which do not create a shower in the calorimeter to those which undergo multiple interactions and consequently deposit up to 80% of their energy. This energy deposit is distributed over a number of crystals. To measure particle energies up to 100 TeV, the readout device has to cover energy deposits from ~5 MeV to about 20 TeV in each individual crystal.

The energy is deposited in the BGO crystals by charged particles through ionization, thereby exciting the BGO lattice. The decay of this excitation produces scintillation light in the crystal which is proportional to the energy deposit and which is radiated isotropically. Due to the difference in the index of refraction at the surfaces, a portion of the light is totally reflected and, thereby, transported to the PMT photocathode, where it is converted into photoelectrons. The amount of light reaching the readout device at the end of the crystal is limited by two factors: 1) the maximum angle at which light is totally reflected at the sides and 2) the maximum angle at which it is not reflected back into the crystal from the readout end. Using an analytical model for the transport of scintillation light through the crystal to the readout device, we determined that about 21% of the light generated is able to exit the crystal at the PMT end.

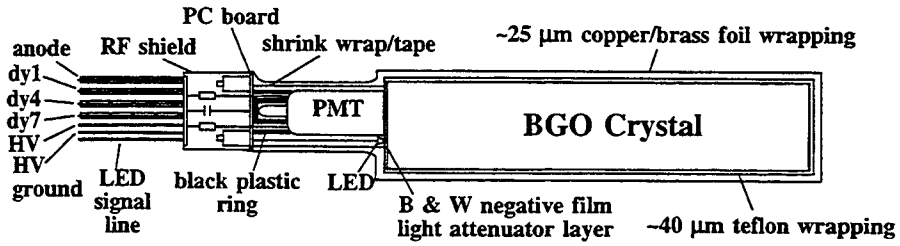

Figure 3: Cross section of a calorimeter subunit

The number of photoelectrons generated depends on, 1) the number and spectrum of photons produced in the BGO crystal for a given energy deposit, 2) the amount of light leaving the crystal at the readout end, 3) the area of the readout surface covered by photocathode and, 4) the quantum efficiency of the photocathode. Table 1 lists the parameters relevant to determining the number of photoelectrons (N) sensed by the R5611 PMT from a single BGO crystal. The number of photons generated for a given energy deposit is listed in the literature as varying between 6000 photons/MeV[11] and 8200 photons/MeV[12]. For the purpose of these calculations, we adopted 7100 photons/MeV. Using these parameters, Table 1 also shows that about 53 photoelectrons are expected per MeV of energy deposit, N = 1222 photoelectrons for a normal incident

minimum ionizing particle (MIP) depositing 23 MeV in a 2.54 cm thick BGO crystal, and ~10^9 photoelectrons are expected for a 20 TeV energy deposit.

Table 1: Parameters for Determining N from a BGO Subunit

Quantum efficiency	13 %
Photocathode size	1.77 cm^2
Area covered by photocathode/area crystal end	0.274
N/MeV	53.1
N/MIP (2.54 cm BGO 23 MeV)	1222
N for 20 TeV	1.06×10^9 (= 170 pC)

BGO crystals have a light decay time of about 300 ns. Our tests show the photocathode of the R5611 is linear to a charge draw of about 7 pC in a short pulse. This requires a light attenuator to bring the anticipated maximum charge of 170 pC at the highest energy deposits down into the linear range. The corresponding signal for minimum ionizing particles (MIP) is attenuated to about 50 photoelectrons. Singly charged particles passing through the glass of the PMT generate about 15 photoelectrons of Cherenkov light. The chosen light attenuation insures that the signal from the BGO crystal dominates. The signal generated by the PMT is read out into 3 ranges, picked off from the dynodes.

3.1.2. The Scintillator Hodoscopes

Each scintillator plane (S1, S2, S3) is composed of two layers mounted at right angles and made of individual segments to form a particle position hodoscope. The width of the segments (~2cm) minimizes the contribution of back-scattered particles to the incident cosmic ray signal and provides a determination of the incident particle trajectory. The length of the segments varies from about 110 cm for S1 to 50 cm for S3 to maintain the 24° opening half angle. The scintillators provide the event trigger and a measure of the incident particle charge. The thickness of each S layer (~1 cm) is selected to minimize Landau fluctuations and total target module thickness while still providing good charge resolution.

Each end of a scintillator segment strip is viewed by a Hamamatsu R5611 photomultiplier through a transition lightguide which provides a good area match between the strip end and the tube photocathode. The anode and dynode from each tube feeds into separate electronic channels to cover the full dynamic range from H to Ni. The top detector (S1) will use Bicron BC-408 as the scintillator, while S2 and S3 will use Ukrainian UPS-923A[13]. The UPS-923A scintillator material has a bulk attenuation length of 3m, a technical attenuation length of 110 cm and light output that is about 25% higher than that of NE114. Each strip is wrapped with an inner layer of foil and an outer black tape layer before being assembled into detector planes.

3.1.3. The Cherenkov Detector

A Cherenkov detector has been included in the ATIC design because of its sensitivity to the direction of the particle's velocity vector. This property allows it to recognize "downward moving" minimum ionizing cosmic ray protons in the presence of the "upward moving" albedo particles. By constructing the Cherenkov detector as a matrix of individual detector elements, we are able to eliminate the signals from albedo particles that do not occur in the element containing the incident cosmic ray's track. To maximize the difference in signal strength between downward and upward moving particles, the top of the radiator is painted black and the sides are aluminized. The use of hexagonal radiators allows packing in a matrix that essentially fills the aperture. The bottoms of the radiators contain a transition region were the shape changes from hexagonal to circular with a diameter of 3 inches to match the photomultiplier tubes. This design is an adaptation of that used in the Sokol experiment[14].

Sokol employed 5 cm thick radiators made of methylmethacrylate (refractive index = 1.48 - 1.5) that were in optical contact with FEU-49 photomultiplier tubes. Results in the laboratory with cosmic ray muons showed that the signal from one downward moving minimum ionizing particle produced approximately 100 photoelectrons, about 15 times larger than the signal produced by upward moving muons. Experience in orbit, showed that about 10 albedo particles were required to equal the signal of an incident proton. This was probably because the albedo particles were primarily electrons that scattered through large angles. Simulations show that particles with signals (corrected for incidence angle) below 3 MIPs can be reliably identified as protons. To raise the mean signal of a cosmic ray proton to 3 MIPs requires that it be accompanied by

approximately 30 albedo electrons, but such a large number of albedo particles passing though a single Cherenkov detector element is highly improbable.

From experience with the Sokol experiment, the heavy ion charge resolution for the Cherenkov detector is given by $\Delta Z = [(.26/Z)^2 + (.2)^2]^{1/2}$. This resolution only separates B from C by 2.1 standard deviations and Ne is separated from Na by only one standard deviation. This poor resolution is due in part to the statistical fluctuations in the Cherenkov signals but it is the non-uniform light collection and the non-uniformity of the photocathode on the FEU-49 that are the main contributors to this loss of resolution. For ATIC we are investigating alternate photomultiplier tubes that would improve the light collection and charge resolution as well as to provide a more compact detector.

3.1.4. The Silicon Matrix Array

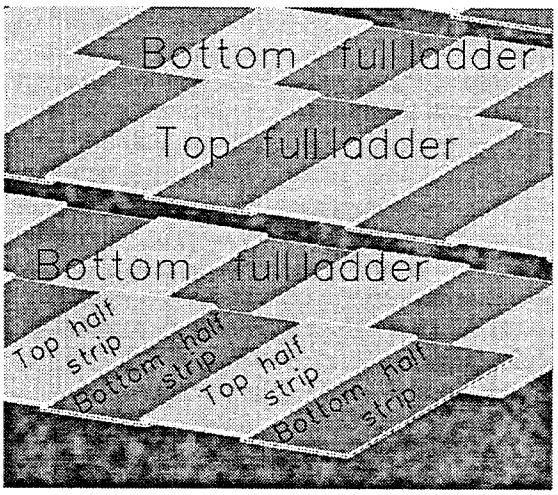

Figure 4: Silicon matrix ladder assembly

The Silicon Matrix Array is a mosaic of fully depleted silicon detectors that fully cover the aperture of the ATIC instrument. Because the Si matrix is the top detector module, it is the largest detector with an area of about 1 m^2. The purposes of the Si detector are to: 1) make an accurate charge identification of the incident cosmic ray from H to Ni, in the presence of albedo; and 2) to contribute to the localization of the incident cosmic ray's trajectory.

The Si matrix is based on a similar matrix built for the ZEUS experiment at DESY. The basic building blocks of the matrix are Si diode detectors with areas of 1.37cm by 1.66 cm. Each detector is fully depleted N-type silicon, 380 μm thick, with a resistivity of 6000 Ω-cm, and operated with a reverse-bias. The detectors are cut from wafers in strips of 4 detectors, and the strips are then mounted in ladder assemblies. As illustrated in Figure 4, each ladder contains 64 Si strips (or 256 detectors) arranged in two rows; one on the top half of the ladder and the other on the bottom half. The strips in the top row are offset so as to cover the gaps between the detectors in the bottom row.

Figure 5 shows a cross section of such a ladder, with the top and bottom half ladders separated to illustrate the placement of the Si strips and the locations of the 2 cm wide multilayer circuit boards. Each ladder is 1 meter long and multiple ladders are arranged next to each other. These are labeled in Figure 4 as "Top full ladder" and the gaps between the strips of adjacent ladders is caused by the placement of the electronic boards. A second plane of ladders is, therefore, mounted below the first plane and offset so as to cover theses gaps ("Bottom full ladder" in Figure 4). Two of the circuit boards will provide bias voltage and detector readout for each half-ladder. The board will be populated with Application Specific Integrated Circuits (ASICs) containing the analog front-end electronics for each detector. These are connected to ADC's and control logic located on the same board at each end. The assembly of ladders forms a self-supporting panel that is 2 cm thick and 1 m on each side. The

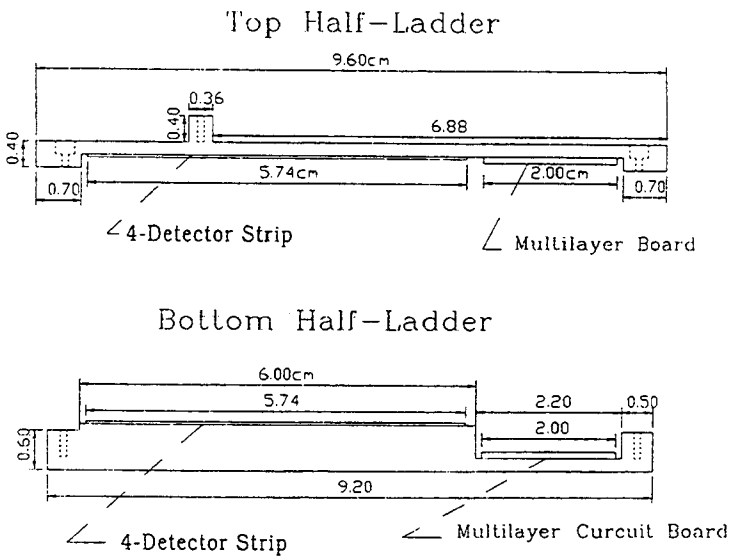

Figure 5: Silicon matrix ladder cross section

matrix will be supported at the edges where it is attached to the ATIC structure. Electrical connections to the ladders will emerge from the ladder ends on ribbon cables that will connect to detector interface modules and the detector control unit that are mounted below the two edges of the matrix at the ladder ends.

Monte Carlo simulations show that, because the individual detector elements are so small, the detector element struck by the incident cosmic ray normally does not also contain an albedo particle track. Sometimes the albedo signal in the struck element can be one MIP but rarely as large as two MIPs. The localization of the incident cosmic ray's trajectory that can be achieved from the calorimeter and the scintillator detectors is somewhat smaller than one Si detector element ($\sigma = 0.54$ at 1 TeV), but often the particle trajectory can only be localized to two or three detector elements. Even in these cases, misidentification of a cosmic ray proton as a Helium nucleus is rare. In addition, the small size of each Si can be used to improve the particle trajectory determination.

The Si matrix also provides a charge measurement to separate the elements up to Ni. Above He this separation is not compromised by the albedo signal because a He cosmic ray gives a signal of 4 MIPs and a Li cosmic ray gives 9 MIPs. The challenge of charge separation higher in the periodic table is that the fractional change in signal decreases with increasing charge so that the Ni, (Z^2), separation is only 7%. The expected elemental resolution for the Si detector is given by $\delta Z = [(0.12/Z)^2 + (0.01)^2]^{1/2}$, so that at Ni, $\delta Z = 1.1\%$.

3.2. The Front End Electronics (FEE)

The front-end electronics system consists of subsystems to 1) form triggers to initiate readout of the instrument, 2) detect and digitize signals from each of the detector arrays, 3) select data from channels with a positive energy deposit (data sparsification), 4) provide in-flight calibration of the detectors and amplifier chains, and 5) collect event rates for diagnostics and flux normalization. In addition, the FEE must provide housekeeping information and must interface to the flight data system described below. The latter is provided by a custom built detector interface module designed for the final front end configuration.

There are two fundamental triggers: a level-1 trigger (pre-trigger) is necessary to stop the acquisition and latch the analog signals on all the detector subsystems, and a master trigger that indicates a good event and initiates a full readout. The level 1 trigger is formed by a coincidence between the S1 and S3 scintillator detectors. This coincidence provides candidate events that are inside the ATIC acceptance geometry, and has an anticipated event rate ~500 Hz. The master trigger is a coincidence between the level 1 trigger and a "shower" in the calorimeter determined by sensing a large signal in the BGO layers. In addition, other coincidence logic will tag "Calibration", "High Z" and "High Energy" events. Such tags might then be used to select highly interesting events for high priority, real time telemetry during the balloon flight.

The requirements on the analog pulse-processing electronics for low power, cost and weight are realized with custom CMOS circuitry. We are evaluating several CMOS VLSI systems for the analog pulse processing electronics. CMOS Application Specific Integrated Circuits (ASICs) that meet our general requirements have been developed and used in accelerator experiments for many years, and are now being integrated into space-based instrumentation. The ASICs, located in the Front End Modules (FEM) provide several functions: charge amplification, analog sampling of the charge amplifier output and analog to digital conversion. ASICs with these functions have been developed by several laboratories (CERN[15], ORNL[16,17], LBNL/CalTech electronics for NASA's Advanced Composition Explorer[18]). Two distinct ASICs will be required for ATIC: one for the Silicon array and one for the PMTs.

Of all the subsystems using photomultiplier tubes, the BGO calorimeter has the most difficult requirements of dynamic range, and hence will drive the specifications for the PMT readout ASIC. Signals in the BGO detectors are taken from three of the photomultiplier tube dynodes as a means of providing, over-all, a wide dynamic range. The basic technique is as follows: The charge amplifier is continuously sampled by two channels of an analog memory formed by switching sampling capacitors on the charge amplifier output. These capacitors hold the voltage of the charge amplifier output at the moment that they sample. After a trigger, an analog sample of the charge amplifier voltage is stored on a third capacitor[16]. The difference between the charge amplifier voltage, both before and after the event, is the desired pulse height which is digitized.

The silicon matrix readout electronics are required to cover a dynamic range of 1100 MIPs. The AMPLEX chip[19,20] is a strong candidate for this task. It is a low noise, very low power (1.5 mW/chan), wide dynamic range system that has been demonstrated to function with input capacitance ~ 100 pF. In order to achieve the required charge resolution, it will be necessary to follow the Amplex output with a dual-gain stage. Each range will be digitized with a low power 12-bit ADC. Required modifications on the Amplex 3b design include a slight reduction in gain, a longer shaping time, and adapting the design to the 1.2 micron CMOS process. Data sparsification will be done after the AMPLEX chip is read out.

3.3. The ATIC Balloon Payload

To turn the ATIC instrument into a flyable balloon payload requires additional support components. Operating at an altitude of about 36 km, the instrument must be able to operate in this near-space environment, i.e. self-powered, capable of transmitting and/or recording the scientific data, and able to function automatically for long periods of time. This section describes the support sub-systems as well as the ATIC flight plans.

3.3.1. Flight Configuration and Schedule

Our engineering studies focused upon three potential flight profiles: a conventional turn-around continental US (CONUS) flight, a LDB flight launched from McMurdo, Antarctica, and a LDB profile using a potential Northern Hemisphere flight path. Each one of these sites imposes different launch weight, power, telemetry, duration, and recovery constraints. To maintain flexibility in the choice of launch sites and to avoid building an instrument with less than optimal science capability, we designed the ATIC charge detectors, carbon target, calorimeter and electronics as modules which can be easily removed or inserted on the support structure. Not only does this design assist in field disassembly and recovery, but it allows us to configure ATIC for a Northern Hemisphere or McMurdo flight with a minimum of effort.

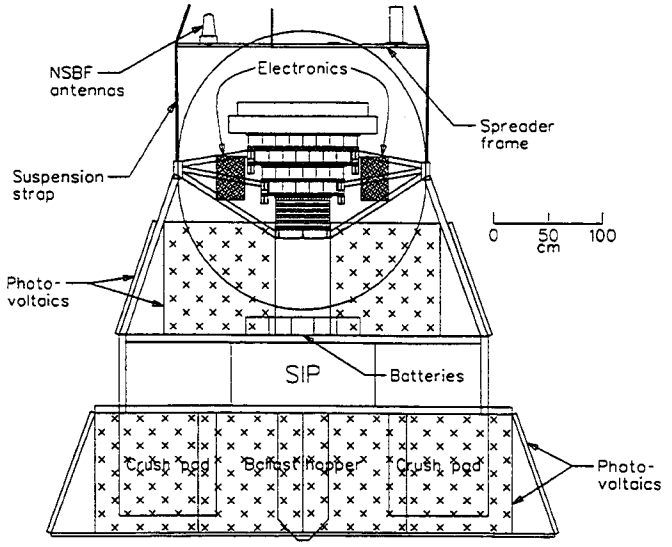

Figure 6: Schematic of the ATIC balloon payload.

A schematic of the payload configuration is shown in Figure 6. The electronic hardware and software associated with the Flight Data System is located in boxes on the sides of the instrument and provides the payload with the ability to collect/record the science data, perform periodic calibrations and react to a partial instrument failure all without direct operator control. A mechanical structure supports the detectors and electronics, transferring the loads to the balloon suspension straps. The required NSBF antennas are mounted above the instrument, and out of the experiment aperture, on a spreader frame that also keeps the suspension straps from contacting and abrading the pressure vessel surface. The instrument and electronics are enclosed within a pressure vessel that maintains a one atmosphere environment. This provides for simplified thermal control and electronic design. Heat is transferred to the pressure vessel surface which then provides a large radiation area. Our thermal calculations show that with a few inches of insulation surrounding the vessel, a relatively uniform temperature of about 20° C can be maintained without an elaborate thermal control mechanism. Power is supplied to the ATIC experiment during LDB flights by photovoltaic (PV) cells. The PV cells are located on all sides, and each side contains the area necessary to power the entire payload. Thus, ATIC does not need a system to orient one side of the payload toward the sun.

We plan to begin our measurement program with a turn-around CONUS flight from Palestine, TX or Ft. Sumner, NM in the Spring of 1999. This flight would allow us to measure the H and He spectrum up to ~10^{13} eV, while providing an opportunity to assess any remaining payload problems relevant to a long duration flight. As a CONUS profile has a high science weight limit, we would plan to fly the baseline Northern Hemisphere configuration. Following recovery and refurbishment, we will embark on a series of LDB flights. Current planning calls for launching from a Northern Hemisphere

site the following year. However, such launches have yet to be proven, and a North American high latitude launch site may not be available. In this case, the ATIC design will allow us to easily reconfigure for a McMurdo Antarctica launch with little impact on the project.

3.3.2. Instrument Control and Data Handling

Figure 7 shows the main components of the flight data system. This system is modularized with each component performing a particular function and communicating across a 10 Mbps ethernet. This modular design provides the ability to easily reconfigure the data system for different flight profiles. Each module has a 486 CPU that handles the "local" functionality and is constructed from commercially available boards, built upon the PC/104 bus, that are low cost, compact, low power, and are widely used in embedded systems. The Flight Control Unit (FCU) coordinates activities among the modules and interfaces with the NSBF SIP (or CIP for turn-around flights) to uplink commands and downlink instrument status frames. Commands are decoded by the FCU which then executes an associated coded directive that may require further commands to be sent to and executed by a subsystem. The FCU polls the data providing modules, such as the Detector Control Unit (which directs the acquisition of data from the detectors upon receipt of a trigger) and the Housekeeping and Power Control Unit (which controls and monitors the payload power system and internal environment) for available data frames. These frames are transferred, time tagged and moved to the Data Archive Unit which stores the data on 4 mm DAT tape. Concurrently, the data frame is also sent to the Telemetry Buffer where it can be held for up to one day. If the payload comes within line-of-sight (LOS) of a telemetry ground station, a command uplinked to the instrument will trigger the Telemetry Transmitter to dump the contents of the buffer through the auxiliary science transmitter at a high bit rate (~320-512 kbps). This provides a mechanism, on LDB flights, for obtaining a significant sample of flight data (for assessing the current instrument performance or as a backup in case the 4 mm data recorders are lost) if ground stations along the LDB path are available or if an aircraft performs underflights. Alternatively, a small sample of the data can be transferred through the FCU and downlinked via TDRSS to a ground system at Palestine, TX where an ATIC supplied workstation will log the data and will function as an FTP and Telenet host, over internet, giving ATIC investigators access to the data and a "tele-presence" in the operations control center.

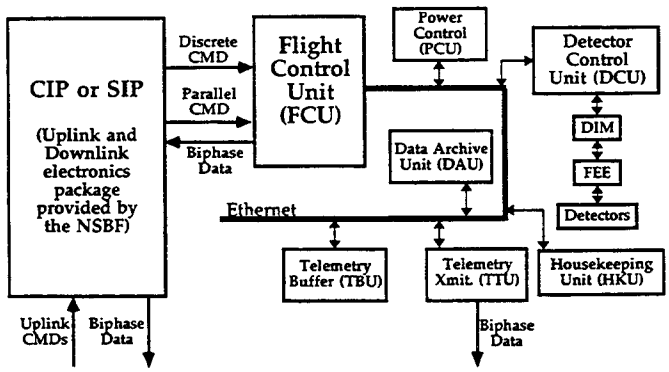

Figure 7: Schematic of ATIC flight data system

The trigger for a nominal ATIC flight will be set with a threshold of ~30 GeV, but will not become very efficient until above 50 GeV. Thus, we would expect to have an average event rate in the ATIC experiment of about 10 per second. With data sparcification incorporated in the detector front end electronics, the corresponding data rate would be about 14 kilobits/second (kbps). The ATIC data stream will also contain housekeeping data, composed of position, universal time, pressure, temperature and voltage information (about once every 5 minutes); a complete readout of all singles and coincidence rates (about once every 30 minutes); and a two point ADC calibration (about once an hour). These extra information frames add about 1% to the average data rate, bringing the total data collected per day to 80 Megabytes (MB). Thus, assuming a 10 day LDB, ATIC should accumulate about 1 GB of information.

3.3.3. Power System

The power system includes the DC / DC converters, relays, circuit breakers, sensors, system controller, DACs and ADCs necessary to supply the required voltages, distribute power to the electronics and detectors as well as to control and monitor the state of the power system. The primary power supply is from lithium cell batteries for short duration CONUS flights and from photovoltaic (PV) arrays for the LDB flights. The PV system has been designed to supply a constant amount of power without the need to orient the payload.

We estimate that ATIC will require about 480 Watts during flight. This assumes the use of low power ASIC circuits, i.e. the Amplex (1.5 mW/channel) discussed above for the Silicon-Matrix and the LBNL/CalTech the ACE Matrix VLSI (14 mW/channel) for the PMTs on the Cherenkov, scintillator and BGO calorimeter detectors. The power required for the flight data system and allied components is about 200 watts.

3.3.4. Structure and Pressure Vessel

The pressure vessel gondola follows a design pioneered by CalTech and manufactured by Irvin Industries, Inc. that consists of two Kevlar fabric hemispherical domes bolted to a 6" tall by 90" diameter aluminum ring using o-ring fitted flanges. An inner bladder composed of polyurethane coated nylon provides the gas-tight seal for the gondola. The advantages of this design are that it is light weight (20 lbs per dome, 125 lbs total), tough and puncture resistant, very thin (~0.06 g/cm^2) and less expensive than equivalent spun aluminum shells. Two such pressure vessels have been delivered to LSU, and one was tested to a pressure of 1.15 atm. with no observable damage.

Mechanical support is provided by honeycomb plates mounted beneath each of the target modules and the calorimeter. The honeycomb plates are supported by aluminum I-beams which are attached to the main structural members. Loads are transferred from the instrument to four load pads mounted on the gondola ring and all loads, including that from the undercarriage/landing frame, are, in turn, transferred to the suspension straps. Thus, the pressure vessel is, in essence, free floating and is not a structural element of the payload. Once all components are taken into account the Northern Hemisphere configuration is expected to weigh about 3,600 lbs. For McMurdo, the T1 target (460 lbs.), and the S2 scintillator (37 lbs.), can be removed, bringing the weight down to about 3,100 lbs.

3.4. The ATIC Data Management Plan

Immediately following the flight, the data tapes made online during the flight and recovered from the payload will be copied, logged and checked for structure and data block defects. The original data tapes will be archived, and a copy will be made for processing. The processing will be performed using programs developed before the flight and incorporate subroutines and calibrations specific to the charge, energy deposit and trajectory analysis. These processed data will be written in a standard data format, such as Common Data Format (CDF), a self-describing, multi-dimensional format which is interoperable across many different platforms and is widely used across the Space Physics Division, and distributed to all collaborating institutions for further analysis. During data analysis each institution will have primary and secondary responsibilities in verifying and refining the data processing algorithms and calibrations. After refinements to the data processing procedures are made, the data will be reprocessed and redistributed for final interpretation. An archive data volume, consisting of processed data and appropriate documentation, will be developed and made available to an appropriate NASA data storage facility.

4. FUTURE PLANS

ATIC is currently funded by NASA in the US to develop, fabricate, integrate, test and fly the balloon payload. Similar support for our European and Korean collaborators is also in place. Currently the team is finalizing the ATIC design details, including choosing and/or modifying appropriate ASIC circuits, producing the mechanical design drawings, developing the Interface Control Documentation, and designing the flight control and data handling software. In addition, construction of the calorimeter detector subunits is under way in Korea and an accelerator calibration of a prototype calorimeter using a subset of these modules is planned for next year. The fabrication effort will significantly increase during 1997 and payload integration is expected to begin in the early summer of 1998. The first ATIC flight is anticipated to be during May, 1999 from a continental US site such as Fort Sumner, NM. This 20 to 30 hour turn-around flight will enable us to investigate the cosmic ray spectrum up to about 10^{13} eV and provide us with an opportunity to flight test the experiment. Following a successful first flight, we then embark on a series of long duration exposures where each flight lasts between 10 and 20 days. Three to four such flights will be necessary for ATIC to obtain statistically significant results for energies to 10^{14} eV.

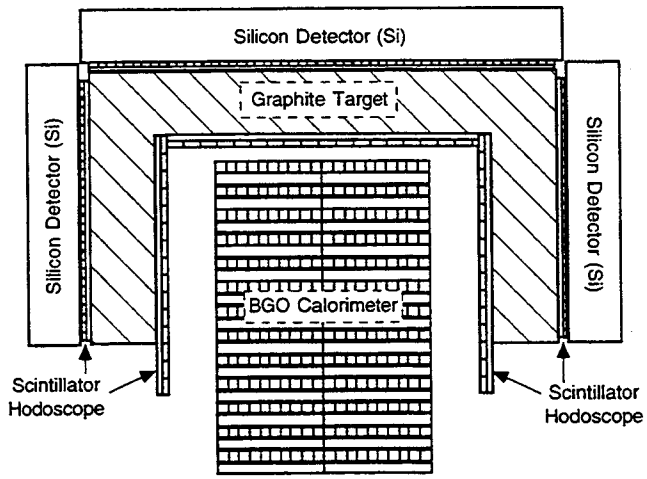

Figure 8: Schematic of the ACCESS instrument concept.

Obtaining measurements over another decade in energy, to $>10^{15}$ eV, requires an exposure factor in excess of 300 m^2-sr -days which can be achieved only by significantly increasing both the geometrical factor and the flight time. A space mission version of the ATIC balloon payload, doubling the number of BGO layers, placing trigger scintillators, silicon matrix detectors and target material on all sides as well as the top of the calorimeter is illustrated in cross section in Figure 8. This experiment, ACCESS, has been proposed to NASA as a new mission concept that would be mounted on the International Space Station (ISS) as a attached payload for a three year exposure.

The measurement technique used by ACCESS is identical to the ionization calorimetry technique discussed above for ATIC. The major difference is that on ACCESS a much deeper calorimeter can be used: 26 layers of 2.5 cm by 2.5 cm by 25 cm long BGO crystals or about 58 radiation lengths vertically. This provides the advantage that higher energy showers from particles incident on the detector up to about 65° from vertical can be contained. Further, the extra layers provide additional points along the shower core to increase the accuracy in determining the incident cosmic ray trajectory. The profile of the core energy deposit as a function of calorimeter depth provides the ability to distinguish between upward and downward going showers. Finally, the outer layers of the calorimeter supplement the thin graphite target in providing the nuclear interactions.

As with ATIC, scintillator hodoscopes provide the event trigger, supplement the trajectory information and provide a redundant measure of the particle charge. The primary charge measuring devices, however, are the Silicon-matrix detectors mounted on all five outer surfaces. These detectors would be constructed of individual elements in a fashion similar to that being developed for ATIC. Thus, the combination of the outer, finely segmented scintillator hodoscope and silicon-matrix provides a two-fold redundancy in rejecting "back-scatter" background tracks.

In space, without a residual atmosphere, we can utilize events at incident angles much larger than are possible with a balloon payload. Thus, in the ACCESS concept, particles can enter from the sides of the instrument as well as the top. This increases the overall geometrical factor of ACCESS to about 0.5 m^2-sr and, combined with a 3 year ISS mission, the total exposure factor would be about 550 m^2-sr-days. Therefore, ACCESS has the potential to provide significant direct measurements of cosmic rays at even higher energies.

5. ACKNOWLEDGMENTS

The ATIC collaboration acknowledges support from NASA under grants NAGW-4577 and NAGW-5064 at LSU, NAGW-4538 and NAG 5-5062 at UMD, DPR S-47414F at NRL, NASA-LEQSF (1994-97-IMP-02-R110044) at Southern and from the European and Korean funding agencies.

6. REFERENCES

1. Seo, E.-S., et al., this conference, paper 2806-17, 1996.
2. Lagage, P. O. & Cesarsky, C. J., Astron. & Astrophys., 118, 223, 1983.
3. Ellison, D. C., et al., Publ. Astron. Soc. Pacific, 106, 780, 1994.
4. Grigorov, N. L., et al, 12th Int. Cosmic Ray Conf. (Tasmania), 5, 1746, 1971.
5. Zatsepin, V.I., 23rd Int. Cosmic Ray Conf. (Calgary), Highlight Papers Volume, p. 439, 1994
6. Zatsepin, V. I., J. Phys. G., 21, L31, 1995.
7. Grigorov, N. L., Cosmic Research (Kosmichekie Issledovaniya), 33, 307, 1995.
8. Ryan, M.J., Ormes, J.F., & Balasubrahmanyan, V.K., Phys. Rev. Letters, 28, 985, 1972.

9. Simon, M., et al., Ap. J. 239, 712, 1980.
10. Ellsworth, R. W., et al., Astrophys. & Space Sci., 52, 415, 1977.
11. Particle Data Group, Phys. Rev. D, 45, No. 11, Part 2, 1992.
12. Knoll, G. F., Radiation Detection and Measurement, 2nd edition, (John Wiley & Sons), p. 231, 1989
13. Bellamy, E.H., Bellettini, G., Budagov, J., et al., Nuc. Instr. & Meth. in Phys. Res., A343, 484, 1994.
14. Grigorov, N.L., Yadernaya fizika, 51, 157, 1990.
15. Anghinolfi, F., et al., IEEE Trans. on Nuc. Sci., 41, No. 4, 1130, 1994.
16. Wintenberg, A. L., et al., IEEE NSS-MIC Conf. Record, 493, 1994.
17. Wintenberg, A. L., Simpson, M. L., Britton, Jr., C. L., et al., IEEE NSS-MIC Conf. Record, 557, 1995.
18. Kleinfelder, S.A., and Kipnis, I., LBNL, Berkeley, CA (private communication) 1996.
19. Beuville, E., et al. Nuc. Instr. & Meth., A288, 157, 1990.
20. Beuville, E., et al., IEEE Trans. on Nuc. Sci., 39, No. 4, 766, 1992.